Single-Crystalline γ-Ga 2 S 3 Nanotubes via Epitaxial Conversion of GaAs Nanowires

Eli Sutter, Jacob S French, Akshay Balgarkashi, Nicolas Tappy, Anna Fontcuberta I Morral, Juan Carlos Idrobo, Peter Sutter

To cite this version:

Eli Sutter, Jacob S French, Akshay Balgarkashi, Nicolas Tappy, Anna Fontcuberta I Morral, et al.. Single-Crystalline γ-Ga 2 S 3 Nanotubes via Epitaxial Conversion of GaAs Nanowires. Nano Letters, 2019, 19 (12), pp.8903-8910. 10.1021/acs.nanolett.9b03783 . hal-02456605

HAL Id: hal-02456605
https://hal.science/hal-02456605

Submitted on 27 Jan 2020

HAL is a multi-disciplinary open access archive for the deposit and dissemination of scientific research documents, whether they are published or not. The documents may come from teaching and research institutions in France or abroad, or from public or private research centers.

L'archive ouverte pluridisciplinaire **HAL**, est destinée au dépôt et à la diffusion de documents scientifiques de niveau recherche, publiés ou non, émanant des établissements d'enseignement et de recherche français ou étrangers, des laboratoires publics ou privés.

Single-Crystalline γ-Ga_2S_3 Nanotubes *via* Epitaxial Conversion of GaAs Nanowires

Eli Sutter,[1] Jacob S. French,[2] Akshay Balgarkashi,[3] Nicolas Tappy,[3]
Anna Fontcuberta i Morral,[3] Juan Carlos Idrobo,[4] and Peter Sutter[2,*]

[1]Department of Mechanical & Materials Engineering, University of Nebraska-Lincoln, Lincoln NE 68588, United States
[2]Department of Electrical & Computer Engineering, University of Nebraska-Lincoln, Lincoln NE 68588, United States
[3]Laboratoire des Matériaux Semiconducteurs, Institut des Matériaux, Ecole Polytechnique Fédérale de Lausanne, Switzerland
[4]Center For Nanophase Materials Sciences, Oak Ridge National Laboratory, Oak Ridge, TN 37831, United States

Abstract

The chemical transformation of nanowire templates into nanotubes is a promising avenue toward hollow one-dimensional (1D) nanostructures. To date, high-quality single crystalline tubes of non-layered inorganic crystals have been obtained by solid-state reactions in diffusion couples of nanowires with deposited thin film shells, but this approach presents issues in achieving single-phase tubes with a desired stoichiometry. Chemical transformations with reactants supplied from the gas- or vapor-phase can avoid these complications, allowing single-phase nanotubes to be obtained through self-termination of the reaction once the sacrificial template has been consumed. Here, we demonstrate the realization of this scenario with the transformation of zincblende GaAs nanowires into single-crystalline cubic γ-Ga_2S_3 nanotubes by reaction with sulfur vapor. The conversion proceeds *via* the formation of epitaxial GaAs-Ga_2S_3 core-shell structures, vacancy injection and aggregation into Kirkendall voids, elastic relaxation of the detached Ga_2S_3 shell, and finally complete incorporation of Ga in a crystalline chalcogenide tube. Absorption and luminescence spectroscopy on individual nanotubes show optoelectronic properties, notably a ~3.1 eV bandgap and intense band-edge and near band-edge emission consistent with high-quality single crystals, along with transitions between gap-states due to the inherent cation-vacancy defect structure of Ga_2S_3. Our work establishes the transformation of nanowires *via* vapor-phase reactions as a viable approach for forming single-crystalline hollow 1D nanostructures with promising properties.

Keywords: Nanowires, Kirkendall effect, cathodoluminescence, electron energy loss spectroscopy, optoelectronics.

*Corresponding author: psutter@unl.edu

High-quality nanostructures, such as nanocrystals, -wires, -tubes, -plates, *etc.*, have been synthesized by a host of different approaches, including for instance colloidal synthesis (nanocrystals),[1,2] vapor-liquid-solid growth (semiconductor nanowires),[3-5] arc evaporation (fullerenes, carbon nanotubes),[6] or chemical vapor deposition (inorganic fullerenes and nanotubes).[7,8] An alternative to such direct synthesis approaches, for example for materials that pose challenges in controlled synthesis or to obtain specific morphologies, such as hollow nanoparticles or -tubes,[9] is the use of a suitable nanostructured template as a substrate for epitaxial growth[10] or as a sacrificial scaffold that can be replaced or transformed *via* chemical reactions.[11] For metal (or metal oxide)[12] nanostructures, galvanic replacement[13] offers a way of obtaining hollow shells of metals, alloys, or metal oxides. Solid-state, gas-, or vapor-phase reactions have been used to convert nanoparticle or nanowire templates into core-shell or hollow structures, notably for oxides and chalcogenides. A classic example is the transformation of metal (*e.g.*, Co, Cd) nanocrystals into hollow metal-oxide or -chalcogenide nanocrystals *via* the nanoscale Kirkendall effect,[14-16] which involves the fast outdiffusion of metal ions through a growing oxide or chalcogenide shell accompanied by the injection, accumulation and coalescence of vacancies in the metallic core, so that the core is completely consumed and a hollow shell results. A similar approach has been used to produce a wide variety of hollow nanostructures,[17-19] including spinel nanotubes formed by reaction of ZnO nanowires with Al_2O_3 shells,[11] cation exchange of ZnO nanowires to TiO_2 nanotubes,[20] transformation of Cu nanowires into CuS_2 and CuS nanotubes,[21] conversion of on-surface Cd nanowires into hemicylindrical CdS tubes,[22] transformation of sacrificial hydroxide ($Co(CO_3)_{0.35}Cl_{0.20}(OH)_{1.10}$) nanorods into Co_9S_8 nanotubes, reaction of β-FeOOH nanorods with ZrO_2 shells to Zr-Fe_2O_3 nanotubes,[23] and the formation of hollow one-dimensional metal oxide shells by oxidation of Ag[24] or Cu[25]

nanowires.

With few exceptions, the hollow nanostructures resulting from chemical transformations are polycrystalline even when starting from single-crystalline templates. Single crystalline nanotubes obtained through chemical transformations were typically obtained by solid-state reactions in diffusion couples, *e.g.*, spinel $ZnAl_2O_4$ by reaction of ZnO nanowires with an atomic-layer deposition (ALD) Al_2O_3 shell or cubic spinel $LiMn_2O_4$ by annealing β-MnO_2 nanotubes coated with LiOH.[26] While these approaches realized attractive properties, such as a well-defined hollow geometry and perfect monocrystallinity, obtaining a single-phase product is complicated by the fact that the solid reactants – typically a sacrificial core and a deposited shell – need to have a precise molar ratio to completely react to the desired product crystal. This can be especially challenging if the template, *e.g.*, a semiconductor nanowire, is tapered with a varying diameter.[27,28] Furthermore, in solid-state reactions it is often unclear which of the solid reactants acts as the template that determines the orientation and crystal phase of the product.[11] Chemical transformations with reactants supplied from the gas- or vapor-phase can avoid these complications. Single-phase nanotubes can be obtained easily since the reaction self-terminates once the sacrificial template has been exhausted. And the crystal phase and lattice orientation of the single-crystalline hollow nanostructures are determined by strict rules of epitaxy over the template crystal at the initial stages of the transformation, *i.e.*, before larger Kirkendall voids appear and the shrinking core detaches from the growing shell/tube.

Here, we demonstrate the realization of this scenario with the transformation of GaAs nanowires into hollow, single-crystalline nanotubes of gallium sulfide (Ga_2S_3). Ga_2S_3 can crystallize in three different phases, monoclinic α-Ga_2S_3,[29,30] hexagonal β-Ga_2S_3,[31,32] and cubic (zincblende) γ-Ga_2S_3.[33,34] This polymorphism is caused by an inherent defect structure, in which

one third of Ga sites are vacant and the stable crystal phases differ in the ordering of the cation sublattice.[35,36] Wide bandgaps close to 3 eV make these materials interesting for optoelectronics, such as light emission and photodetection in the short-wavelength visible range,[37,38] as well as second-harmonic generation[37,39] benefitting from high laser-induced damage thresholds.[39] Light emission is often governed by defect levels, *e.g.*, due to the abundant cation vacancies, and thus occurs across a wider range of the visible spectrum.[36-38,40-42] We show that zincblende GaAs nanowires exposed to sulfur vapor transform into GaAs-Ga_2S_3 core-shell nanowires, followed by the retraction of the cores by injection and coalescence of vacancies into Kirkendall voids, and ultimately the complete reaction of Ga from the GaAs cores, congruent desorption of As, and formation of hollow Ga_2S_3 nanotubes. The templating by high-quality GaAs nanowires enables the formation of single-crystalline zincblende γ-Ga_2S_3 tubes, whose lattice structure – down to the arrangement of crystal twins – is entirely inherited from the template crystals. Optical absorption measurements on individual Ga_2S_3 nanotubes by electron energy loss spectroscopy in monochromated scanning transmission electron microscopy (STEM-EELS) identify a bandgap of 3.1 eV. Nanoscale luminescence spectroscopy shows band-edge emission, intense near band-edge luminescence at ~460 nm (*i.e.*, ~2.67 eV photon energy), and additional light emission between ~560 – 750 nm from transitions involving defect states in the gap. These characteristics document the promising optoelectronic properties of single-crystalline Ga_2S_3 nanotubes.

The approach for preparing high-quality zincblende γ-Ga_2S_3 nanotubes is summarized in Figure 1. Single-crystalline GaAs nanowires grown by self-catalyzed molecular beam epitaxy using Ga drops as catalysts (see Methods for details) are used as templates for the epitaxial conversion to hollow nanotubes. Fig. 1 (a) shows a transmission electron microscopy (TEM) image of one of the GaAs nanowires. The striped contrast stems from a sequence of twins in the

zincblende GaAs nanowires.[43] The darker liquid Ga catalysts appear as homogeneous spherical caps without any internal contrast.[44] Electron diffraction (Fig. 1 (a), inset) demonstrates that the nanowires are single crystalline with symmetry axis oriented along the [111] direction.

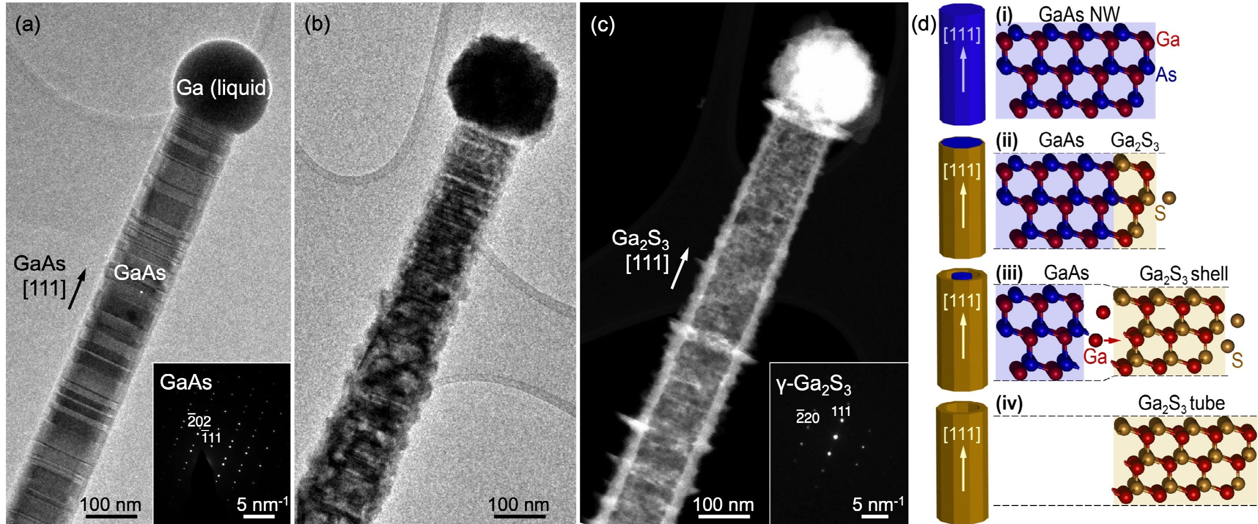

Figure 1. Single-crystalline Ga_2S_3 nanotubes by solid-state transformation of a sacrificial GaAs nanowire template. (a) Zincblende GaAs nanowire grown by MBE using Ga catalyst drops. The nanowire axis is aligned along the GaAs [111] direction. Inset: Selected-area electron diffraction pattern. **(b)** GaAs-Ga_2S_3 core-shell nanowire following sulfurization of a GaAs nanowire for 15 min. at 620°C (sulfur vapor pressure, p~10^{-4} Torr). **(c)** Single-crystalline hollow γ-Ga_2S_3 nanotube obtained by complete transformation of the sacrificial GaAs nanowire template after annealing in sulfur for 60 min. at 620°C. Inset: Selected-area electron diffraction pattern indexed to cubic (zincblende) γ-Ga_2S_3. The tube axis is aligned with the Ga_2S_3 [111] direction. Note: Panels (a) – (d) do not show the same nanowire/tube. **(d)** Schematic reaction sequence: **(i)** Sacrificial GaAs nanowire template; **(ii)** Initial stage of solid-state transformation during sulfur exposure: Formation of a strained epitaxial Ga_2S_3 shell on the GaAs nanowire core; **(iii)** Progressive outdiffusion and reaction of Ga from the GaAs core, causing the detachment and elastic relaxation of the thickening Ga_2S_3 shell; **(iv)** Final stage: Single-crystalline (zincblende) γ-Ga_2S_3 nanotube.

GaAs nanowires were progressively transformed by reaction with sulfur vapor at different temperatures (see Methods), following the sequence of reaction steps illustrated schematically in Fig. 1 (d). The initial sulfur exposure converted the near-surface region of the nanowires into a thin epitaxial Ga_2S_3 shell that is strained within the cylindrical interface to the GaAs lattice (Fig. 1 (d), (ii)). Further exposure to sulfur drives the diffusion of Ga ions and vacancies through this shell, causing a thickening of the Ga_2S_3 and its detachment from the

shrinking GaAs core (Fig. 1 (d), (iii)), thus lifting epitaxial constraints and allowing the Ga_2S_3 shell to relax to its intrinsic lattice parameters. The thickening of the shell continues until the entire GaAs core has been consumed. At this final stage, Kirkendall voids have coalesced to a hollow core surrounded by a single-crystalline γ-Ga_2S_3 nanotube (Fig. 1 (d), (iv)). Representative images of stages (iii) and (iv) are shown in Fig. 1 (b) and Fig. 1 (c), respectively (for different nanowires/tubes). While we focus on individual nanostructures in our in-depth structural characterization and in the probing of optoelectronic properties, the exemplary structures reflect and represent the properties found across larger ensembles, as shown in Fig. S1. Fig. 1 (b) illustrates the GaAs-Ga_2S_3 core-shell nanowire morphology resulting from a partial sulfurization of a GaAs nanowire. Selected-area (Fig. 2, see discussion below) and nanobeam electron diffraction (Fig. S2) show the coexistence of a single-crystalline GaAs core and γ-Ga_2S_3 shell, both unstrained. The high-angle annular dark field (HAADF) STEM image in Fig. 1 (c) shows the final stage, *i.e.*, a hollow Ga_2S_3 nanotube, here with outer diameter of 150 nm and wall thickness of ~25 nm. Note the protrusions from the outer surface of the tube wall, which indicate accelerated Ga_2S_3 growth along parts of the wall suggesting Ga mass transport along the tube axis prior to migration across the Ga_2S_3 layer. Local electron diffraction (Fig. 1 (c), inset) and nanobeam electron diffraction line scans (Fig. S3) show that the nanotubes are single-crystalline with diffraction patterns matching the structure of unstrained (zincblende) γ-Ga_2S_3 along the entire length.

While prior work showed alternative mechanisms for the hollowing-out of nanoscale structures, such as shell-induced Ostwald ripening,[45] several observed characteristics support the assignment of the process to a nanoscale Kirkendall effect. Although we were not able to obtain a direct comparison of the same nanowire/tube before and after the sulfurization reaction,

ensemble statistics show the increase in diameter from the initial GaAs nanowire template to the final Ga_2S_3 nanotube expected due to void formation in the core and Ga mass conservation. For example, thin GaAs nanowires with diameters of 32-35 nm are converted to Ga_2S_3 nanotubes with diameters of 38-40 nm. Wires with varying degree of conversion at different positions (quantified *via* the projected void fraction in TEM images) show a constant inner diameter of the Ga_2S_3 tube, and an outward sidewall growth with a wall thickness correlated with the amount of reacted core material (Fig. S4), which are clear indicators for a preferential outdiffusion of Ga. Finally, the observed protrusions attached to the outer tube wall are also consistent with a Kirkendall mechanism.

While it is plausible that the initially ultrathin shell is strained in the interface plane to the lattice parameter of the GaAs template (Fig. 1 (d), stage (ii)), we were unable to identify conditions under which this state is realized experimentally and the strained ultrathin Ga_2S_3 shell would be detectable in electron diffraction (Fig. S8). The analysis of Fig. S4 (c)-(e) suggests the formation of a thin Ga_2S_3 shell during the initial reaction with sulfur without substantial Ga mass transport, with vacancy injection and hollowing out of the core beginning later. Figure 2 summarizes the diffraction analysis of the strain relaxation of the Ga_2S_3 shell after it detaches from the GaAs core *via* insertion of Kirkendall voids between core and shell (Fig. 1 (d), stage (iii)). TEM (Fig. 2 (a)) and STEM images (Fig. 2 (b)) show a clear separation between the core and shell (see Fig. 2 (b), inset). Selected-area electron diffraction patterns of this monocrystalline core-shell nanowire along two different zone axes ($[11\bar{2}]$, Fig. 2 (c); $[101]$, Fig. 2 (d)) consist of a superposition of two zincblende single-crystal patterns originating from GaAs (lattice constant 5.565 Å) and γ-Ga_2S_3 (5.181 Å), respectively. Comparison with simulated diffraction patterns of Ga_2S_3 and GaAs (Figs. 2 (c'), (d')) shows an excellent match when assuming unstrained but

aligned GaAs and Ga_2S_3 crystal lattices. The epitaxial alignment is evident from the well-defined offset directions of the two sets of diffraction spots, with larger reciprocal spacings corresponding to γ-Ga_2S_3 (Fig. 2 (c, c'), Fig. 2 (d, d'); HRTEM: Fig. 2 (e)-(f)). Linear arrays of nanobeam electron diffraction patterns obtained along the nanowire show that these characteristics – relaxed, lattice-aligned monocrystalline core and shell – are obtained across

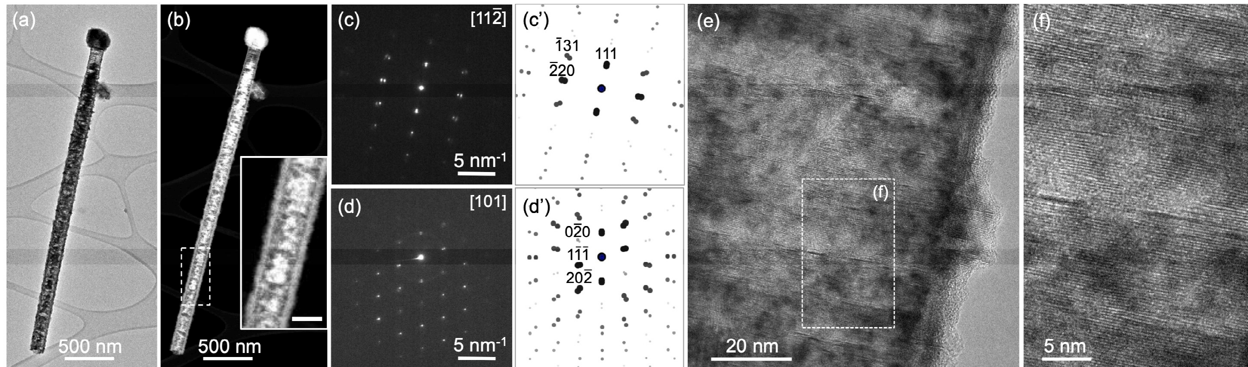

Figure 2. Core-shell nanowires consisting of detached, unstrained GaAs templates and Ga_2S_3 shells. (a) TEM and **(b)** HAADF-STEM of a partially reacted core-shell nanowire (stage (iii), Fig. 1 (d)) following exposure to sulfur (vapor pressure, p ~10^{-4} Torr) at 620°C. The inset in (b) shows a magnified view of the dashed area. **(c), (d)** Selected-area electron diffraction along two different zone axes, $[11\bar{2}]$ (c) and [101] (d), with superimposed patterns of GaAs and relaxed Ga_2S_3 showing the epitaxial relationship between the GaAs core and the single crystalline Ga_2S_3 shell. **(c'), (d')** Simulated diffraction patterns of epitaxially aligned GaAs and Ga_2S_3, both with their equilibrium (unstrained) lattice constants. **(e), (f)** HRTEM images of the GaAs-Ga_2S_3 core–shell nanostructure.

the entire core-shell structure (Fig. S2). The only exception is the nanowire tip, where the Ga catalyst drop is typically converted into polycrystalline cubic Ga_2S_3.

Further reaction with sulfur vapor converts these core-shell nanowires into hollow, single-crystalline γ-Ga_2S_3 nanotubes (Fig. 1 (d), stage (iv)). The final structure and morphology resulting from the sulfurization reaction are documented in Figure 3. TEM images of a representative Ga_2S_3 nanotube (Figs. 3 (a), (b)) and HAADF-STEM (Fig. 3 (c)) clearly show the hollow core and uniform ~25 nm sidewall, the latter with darker and brighter contrast in TEM and HAADF-STEM, respectively, due to its larger overall projected thickness of solid Ga_2S_3. The outer surface of the tube now appears more corrugated than that of the core-shell wire shown

in Fig. 2, primarily due to local differences in the thickening of the Ga_2S_3 shell producing characteristic arrays of fin-like protrusions. Nevertheless, the hollow tubes obtained by reaction

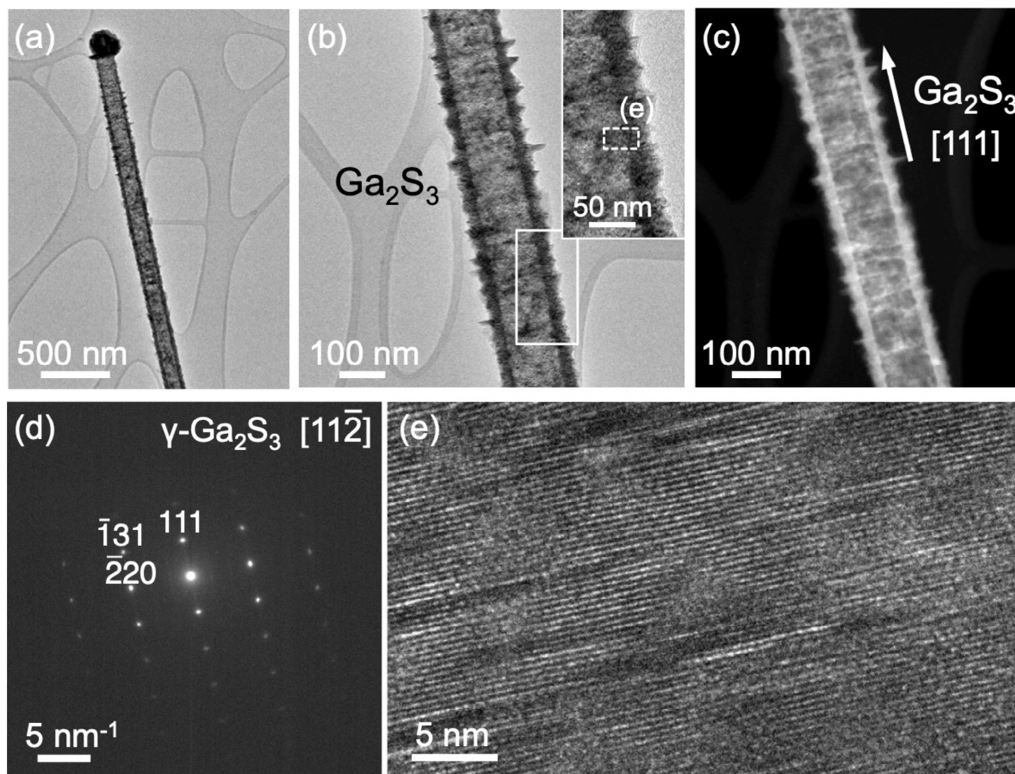

Figure 3. Single crystalline Ga_2S_3 nanotubes by sulfurization of sacrificial GaAs nanowire templates. (a) TEM image of a characteristic Ga_2S_3 nanotube formed during sulfurization at 620ºC for 1 hour (sulfur vapor pressure, p ~10^{-4} Torr). **(b)** Higher magnification TEM and **(c)** HAADF-STEM images of a section of the nanotube in (a). The inset in (b) shows a magnified view of the marked rectangular area. **(d)** Electron diffraction pattern along the [11$\bar{2}$] zone axis, showing single crystalline cubic γ-Ga_2S_3. **(e)** HRTEM image of the sidewall of the Ga_2S_3 nanotube, marked in the inset of (b).

with sulfur above 600°C are invariably single crystalline and aligned along the [111] direction, as dictated by the templating effect of the [111]-oriented GaAs nanowires. This is shown by selected-area electron diffraction (Fig. 3 (d)) and corroborated by series of nanobeam diffraction patterns obtained along the tubes (Fig. S3), which now contain only a single set of spots indexed to monocrystalline γ-Ga_2S_3. The diffraction spots from GaAs observed in the core-shell structures at earlier reaction stages (Fig. 2) are now absent, confirming the complete transformation of the GaAs core into a Ga_2S_3 nanotube. No sulfur is detectable, as expected after

cooling of the reacted nanotubes under vacuum, *i.e.*, at negligible S vapor pressure. High-resolution (HR) TEM illustrates the high crystalline quality of the tube (Fig. 3 (e)) and shows a sequence of twins as the predominant defect in the tubes (Fig. S5). The similarity of the twinning patterns in the initial zincblende GaAs nanowires and the Ga_2S_3 nanotubes suggests that the sulfurization reaction transcribes not only the lattice structure and orientation, but even the sequence of planar defects from the GaAs nanowire templates to the final Ga_2S_3 nanotubes (Figs. S5-S7).

Whereas ordered monocrystalline γ-Ga_2S_3 nanotubes are obtained by sulfurization at temperatures between 600-620°C, lower reaction temperatures still produce hollow nanotubes, albeit consisting of polycrystalline γ-Ga_2S_3. Figures S9 and S10 illustrate the morphology of representative GaAs nanowires after reaction with sulfur vapor at 450°C. TEM imaging and electron diffraction (Fig. S9 (b)) demonstrate that the GaAs nanowires remain intact after the brief sulfur exposure at these conditions. The liquid Ga drop at the tip undergoes a drastic change, and after sulfurization is replaced by a thick shell surrounding a hollow core. Electron diffraction (Fig. S9 (b')) identifies its structure and that of the thin shell on the nanowires as cubic Ga_2S_3. Similar morphologies were observed after brief sulfurization at temperatures between 350°C and 550°C. Longer exposures allowed us to access the entire sequence of regimes shown in Fig. 1 (d), however without achieving a long-range ordered monocrystalline structure. Note that the exposure times are correlated to the GaAs nanowire diameter, *i.e.*, thinner GaAs nanowires progress toward the final hollow tube morphology faster than thicker wires (Fig. S11). Reactions at higher temperatures (550°C) show etching of the GaAs core preferentially along [110] directions, and the formation of smooth, polycrystalline γ-Ga_2S_3 shells and nanotubes (Figs. S11- S13).

Single-crystalline Ga_2S_3 nanotubes formed by reaction with sulfur may be of interest for applications in optoelectronics (*e.g.*, photodetection[37] and short wavelength light emission), second harmonic generation,[39] and sensing.[38] To explore this potential, we probed the optoelectronic properties of individual high-quality γ-Ga_2S_3 tubes using nanometer-scale STEM-EELS combined with cathodoluminescence spectroscopy in STEM (STEM-CL) and scanning electron microscopy (SEM-CL). In contrast to other phases of Ga_2S_3, particularly monoclinic α-Ga_2S_3 (Refs. 38,40,46), the optoelectronic properties of cubic γ-Ga_2S_3 remain poorly understood. Reported absorption measurements on single crystals showed a bandgap of ~2.74 eV, smaller than that reported for the other Ga_2S_3 phases (3.0-3.4 eV).[36,38,40] Recent CL measurements on thin γ-Ga_2S_3 flakes showed pronounced defect luminescence centered between 550-800 nm – far from the band-edge emission expected below ~450 nm – with a temperature-dependent intensity that was strongly attenuated at room temperature.[37]

Figure 4 summarizes measurements of the optoelectronic properties on individual single-crystalline γ-Ga_2S_3 nanotubes formed by sulfurization of GaAs nanowire templates at 620°C (as shown in Fig. 3). Local absorption measurements by monochromated STEM-EELS (Fig. 4 (a)-(b)) show a narrow zero-loss peak (full-width at half maximum: FWHM ~ 68 meV) and a clear onset of increased losses due to interband transitions, allowing us to extract a bandgap E_g = 3.1 eV (close to the reported value for monoclinic α-Ga_2S_3).[38] Some of the EELS spectra show an additional absorption onset in the gap, consistent with sub-bandgap (defect) emissions in luminescence. Local luminescence was measured by STEM-CL between 300-1000 nm (Figs. 4 (c)-(f)), and by SEM-CL with extended ultraviolet range down to 200 nm (Figs. 4 (g)-(i)). The spectra generally show contributions from band-edge luminescence centered near 400 nm (3.1 eV), along with intense near band-edge emission and additional radiative transitions with

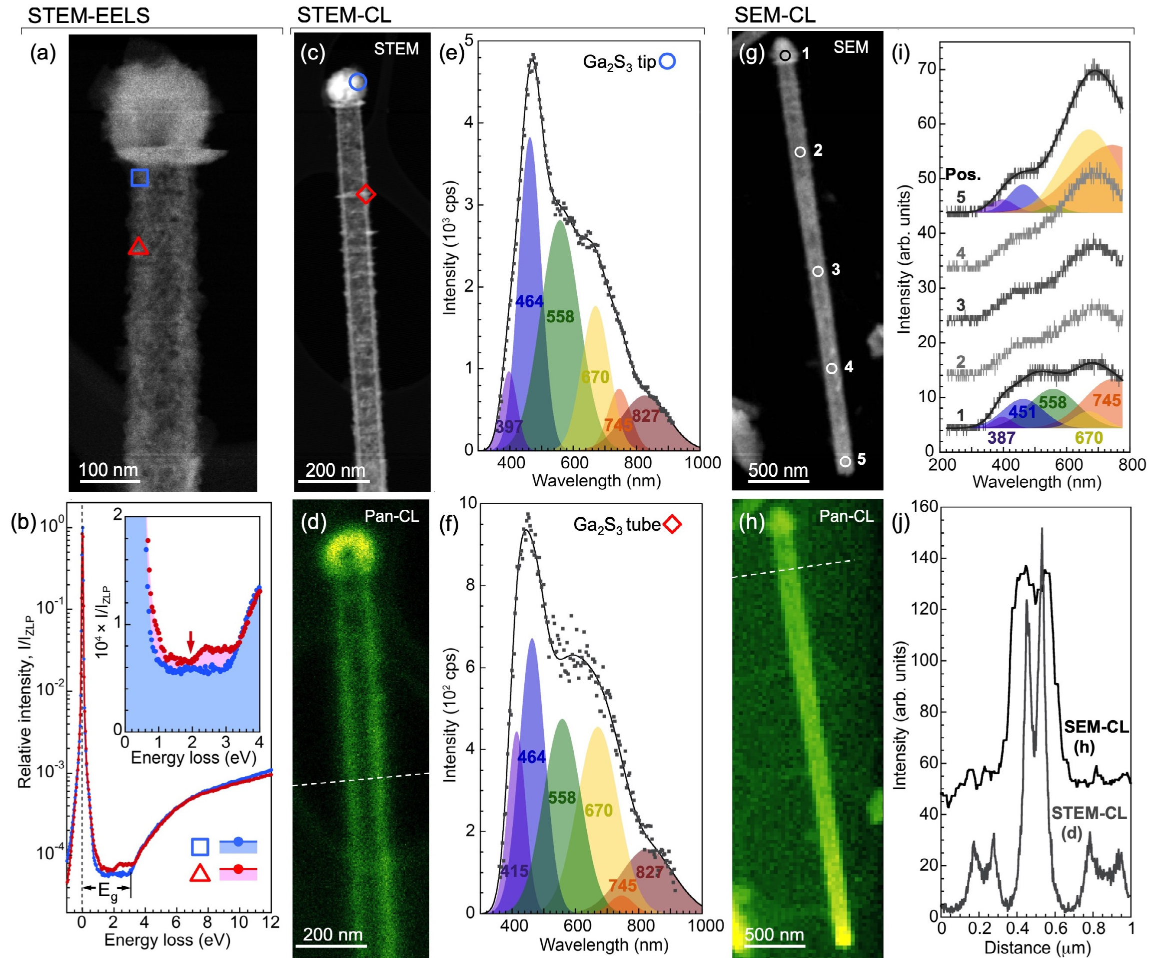

Figure 4. Optoelectronics of individual single-crystalline Ga_2S_3 nanotubes. (a)-(b) Single nanotube absorption measurements by monochromated STEM-EELS at 300 K. (a) HAADF-STEM image of a typical Ga_2S_3 nanotube. **(b)** Monochromated STEM-EELS spectra obtained at two locations of the nanotube, marked in (a). FWHM of the zero-loss peak (ZLP): 68 meV. Measured bandgap: E_g = 3.1 eV. Inset: Zoomed spectra in the bandgap region, showing additional absorption from gap states (red arrow). **(c)-(f) STEM cathodoluminescence, measured at 300 K. (c)** HAADF-STEM image of a typical Ga_2S_3 nanotube. **(d)** Panchromatic STEM-CL map, showing predominant photon emission from the Ga drop at the tip (transformed by sulfurization to Ga_2S_3) as well as the Ga_2S_3 nanotube sidewalls. **(e)** STEM-CL spectrum obtained with the exciting electron beam positioned at the Ga_2S_3 tip (blue circle in (c)). **(f)** STEM-CL spectrum from the Ga_2S_3 nanotube sidewall (red diamond in (c)). Colored regions in (e) and (f) represent components of a Gaussian peak shape analysis of the CL spectra, with center wavelengths of the Gaussians as indicated (in nm). **(g)-(i) SEM cathodoluminescence, measured at T = 10 K. (g)** SEM image of a Ga_2S_3 nanotube. **(h)** Panchromatic SEM CL map showing enhanced emission from the tip and wire end. **(i)** SEM-CL spectra obtained at positions along the Ga_2S_3 nanotube marked in (g). Colored regions represent components of a Gaussian peak shape analysis of the CL spectra, with center wavelengths fixed at the same values used in the deconvolution of the STEM-CL spectra shown in (e) and (f), except for the highest energy (band-edge) peaks, which were shifted to lower wavelength to account for bandgap widening between 300 K and 10 K. **(j)** Comparison of STEM-CL and SEM CL intensity profiles, obtained along the dashed lines in the panchromatic maps shown in (d) and (h), respectively. Both intensity profiles show enhanced emission from the sidewall and a dip near the center of the hollow Ga_2S_3 nanotubes.

energies below E_g. These different features were extracted by least-squares fits to a minimal set of Gaussian components, which were used for the analysis of all luminescence spectra.

Panchromatic luminescence maps in STEM-CL show intense emission from the sulfurized Ga drop at the nanotube tip as well as from the tube sidewalls, where the projected volume of Ga_2S_3 excited by the electron beam is largest (Fig. 4 (c), (d)). Resolved features such as the fin-like protrusions along the tube surface attest to the high spatial resolution achieved in these measurements (Fig. 4 (d)). Besides the band-edge luminescence, STEM-CL spectra obtained both at the tip and sidewalls show a dominant peak due to near band-edge luminescence (centered at λ = 464 nm, 2.67 eV) and prominent green (558 nm) and red (670 nm) defect luminescence. The defect emissions are consistent with photoluminescence peaks of γ-Ga_2S_3 prepared by sulfurizing bulk GaAs,[41] and the red emission reported for cubic Ga_2S_3 flakes grown on mica.[37] The green luminescence has been attributed to transitions from the conduction band minimum or shallow donor levels to an acceptor level due to excited V_{Ga}^{+2} vacancies positioned ~0.7 eV above the valence band edge;[41,47] the red emission was assigned to transitions from a deep donor level to the V_{Ga}^{+2} acceptor.[41] While showing similar defect emission components, our luminescence spectra contrast in two key aspects with previous reports:[37,41] (i) they show bright band-edge and near band-edge luminescence; and (ii) STEM-CL measurements at variable temperature show the emission intensity remaining nearly unchanged across a wide temperature range between 110 K and room temperature.

Panchromatic SEM-CL maps (Fig. 4 (g), (h)) are in excellent agreement with measurements using high-energy electron excitation in STEM and show the same intensity distribution with maxima at the tube walls and a dip over the hollow core (Fig. 4 (j)). SEM-CL spectra obtained at T = 10 K at different positions along single-crystalline γ-Ga_2S_3 nanotubes

(Fig. 4 (i), Fig. S14) were fitted with the same overall line shape observed in STEM-CL, *i.e.*, deconvoluted into the same Gaussian components assigned to band-edge and defect luminescence. To account for the bandgap widening at low temperature, the Gaussians representing the band-edge peaks were blue-shifted by ~80 meV relative to the same fit components in the room-temperature STEM-CL spectra. With its extended spectral range, SEM-CL clearly confirms the absence of short-wavelength emissions beyond those found in STEM-CL.

In conclusion, we have demonstrated a process – based on reactions with vapor- or gas-phase species – for the controlled conversion of sacrificial nanowire templates into high-quality single-crystalline nanotubes, exemplified here by the transformation of GaAs nanowires into γ-Ga_2S_3 nanotubes by reaction with chalcogen (sulfur) vapor. Similar to previous approaches that used diffusion couples of nanowires and deposited solid shells to form hollow tubes *via* solid-state reactions, the method reported here combines structural templating by nanowires with hollowing by the nanoscale Kirkendall effect to create single-crystalline nanotubes. But in contrast to solid diffusion couples, where a precisely tuned local molar ratio of the reactants is crucial and which therefore face limitations, *e.g.*, in case of inhomogeneous diameters of the starting nanowires, our reactions with species supplied from the vapor- or gas-phase are self-teminating and robust in providing single-phase tubes. For the particular system considered here, the transformation of GaAs nanowires into Ga_2S_3 nanotubes, our results establish several interesting structural features, notably the selection among several known Ga_2S_3 phases of a specific (γ, zincblende) polymorph matching the structure of the zincblende GaAs template, and the transcription of other characteristics such as the arrangement of twins from the nanowire template. Nanoscale luminescence spectroscopy on individual γ-Ga_2S_3 nanotubes shows, in

addition to the ubiquitous transitions between gap states due to the inherent defect structure with abundant cation vacancies, strong band-edge and near band-edge emissions, providing further support for the high quality of these hollow nanostructures and paving the way for their application in areas such as optoelectronics or sensing.

MATERIALS AND METHODS

GaAs nanowires were synthesized at EPFL by molecular beam epitaxy as described in detail elsewhere.[48,49] Briefly, Ga-catalyzed growth was carried out in an ultrahigh vacuum reactor at 630°C on GaAs substrates covered with SiO_2. As-grown nanowires on the original substrates were transferred through air to UNL, where they were exposed to sulfur vapor in a quartz-tube reactor with two temperature zones. For the sulfurization reactions, sulfur powder (99.9995%, Alfa Aesar) was loaded into a quartz boat and placed in the center of the first (upstream) zone and samples were positioned in the second zone. The reactor was evacuated by a mechanical pump and $Ar:H_2$ (ratio 98:2) carrier gas was introduced at 50 sccm flow rate and 20 mTorr pressure. GaAs nanowire sulfurization was carried out at different sample temperatures between 350°C and 650°C. Heating the sulfur reservoir to a temperature of 80°C established a vapor pressure of ~4×10^{-4} Torr.[50] To compare the effects of sulfur vapor pressure, three different sulfur reservoir temperatures (80°C, 120°C, and 170°C) corresponding to sulfur vapor pressures between 4×10^{-4} Torr and 0.72 Torr were used. Constant temperatures during the reaction were ensured by ramping the two furnace zones so as to reach the chosen settings at the same time. Sulfur exposure time ranged between 15 minutes and 4 hours (as indicated in the paper). Upon completion the system naturally cooled to room temperature.

The morphology of the GaAs nanowires after sulfurization was investigated at UNL by TEM, HAADF-STEM, and nanobeam electron diffraction in an FEI Talos F200X field-emission microscope. For these investigations the nanowires/tubes were dispersed on amorphous C films supported by Cu grids. The optoelectronic properties of individual Ga_2S_3 nanotubes were characterized by both local absorption and luminescence spectroscopy. Absorption was measured by mapping the onset of losses in the low-loss region by monochromated STEM-EELS in a Nion Hermes microscope (at Oak Ridge) at 60 keV electron energy and 0.12 nm probe size. Cathodoluminescence (CL) measurements were performed in STEM mode (STEM-CL at UNL) and SEM mode (SEM-CL at EPFL). STEM-CL was performed using a Gatan Vulcan CL holder at room temperature and 200 keV electron energy, at an incident beam current between 300-400 pA. Local STEM-CL spectra were acquired by positioning the focused electron beam excitation at chosen locations and integrating the spectrometer output detected by a Si CCD array detector for 10-20 seconds. SEM-CL measurements were carried out at T = 10 K in an Attolight system at 5 keV electron energy and beam currents of 5-20 nA.

ACKNOWLEDGEMENTS

The authors thank E. Uccelli for contributions to the synthesis of high-quality GaAs nanowire templates. This work was supported by the National Science Foundation, Division of Materials Research, Solid State and Materials Chemistry Program under Grant No. DMR-1607795. A.F. i M. acknowledges support from the Swiss National Science Foundation (Projects No. 40B2-0_176680 and 200020_137648) and from the European Union through Horizon-2020 (project LIMQUET).

References:

1. Turkevich, J.; Stevenson, P. C.; Hillier, J. A study of the nucleation and growth processes in the synthesis of colloidal gold. *Discussions of the Faraday Society* **1951,** 11, 55-75.
2. Murray, C. B.; Norris, D. J.; Bawendi, M. G. Synthesis and characterization of nearly monodisperse CdE (E = sulfur, selenium, tellurium) semiconductor nanocrystallites. *Journal of the American Chemical Society* **1993,** 115, 8706-8715.
3. Wagner, R. S.; Ellis, W. C. Vapor-Liquid-Solid Mechanism of Single Crystal Growth. *Applied Physics Letters* **1964,** 4, 89-90.
4. Morales, A. M.; Lieber, C. M. A Laser Ablation Method for the Synthesis of Crystalline Semiconductor Nanowires. *Science* **1998,** 279, 208-211.
5. Güniat, L.; Caroff, P.; Fontcuberta i Morral, A. Vapor Phase Growth of Semiconductor Nanowires: Key Developments and Open Questions. *Chemical Reviews* **2019,** 119, 8958-8971.
6. Kroto, H. W.; Heath, J. R.; O'Brien, S. C.; Curl, R. F.; Smalley, R. E. C60: Buckminsterfullerene. *Nature* **1985,** 318, 162-163.
7. Tenne, R.; Margulis, L.; Genut, M.; Hodes, G. Polyhedral and cylindrical structures of tungsten disulphide. *Nature* **1992,** 360, 444-446.
8. Feldman, Y.; Wasserman, E.; Srolovitz, D. J.; Tenne, R. High-Rate, Gas-Phase Growth of MoS_2 Nested Inorganic Fullerenes and Nanotubes. *Science* **1995,** 267, 222-225.
9. Wang, X.; Feng, J.; Bai, Y.; Zhang, Q.; Yin, Y. Synthesis, Properties, and Applications of Hollow Micro-/Nanostructures. *Chemical Reviews* **2016,** 116, 10983-11060.
10. Goldberger, J.; He, R.; Zhang, Y.; Lee, S.; Yan, H.; Choi, H.-J.; Yang, P. Single-crystal gallium nitride nanotubes. *Nature* **2003,** 422, 599-602.
11. Jin fan, H.; Knez, M.; Scholz, R.; Nielsch, K.; Pippel, E.; Hesse, D.; Zacharias, M.; Gösele, U. Monocrystalline spinel nanotube fabrication based on the Kirkendall effect. *Nature Materials* **2006,** 5, 627-631.
12. Oh, M. H.; Yu, T.; Yu, S.-H.; Lim, B.; Ko, K.-T.; Willinger, M.-G.; Seo, D.-H.; Kim, B. H.; Cho, M. G.; Park, J.-H.; Kang, K.; Sung, Y.-E.; Pinna, N.; Hyeon, T. Galvanic Replacement Reactions in Metal Oxide Nanocrystals. *Science* **2013,** 340, 964-968.
13. Xia, X.; Wang, Y.; Ruditskiy, A.; Xia, Y. 25th Anniversary Article: Galvanic Replacement: A Simple and Versatile Route to Hollow Nanostructures with Tunable and Well-Controlled Properties. *Advanced Materials* **2013,** 25, 6313-6333.
14. A.D. Smigelskas; Kirkendall, E. O. Zinc Diffusion in Alpha Brass. *Transactions of the AIME* **1947,** 171, 140-142.
15. Yin, Y.; Rioux, R. M.; Erdonmez, C. K.; Hughes, S.; Somorjai, G. A.; Alivisatos, A. P. Formation of Hollow Nanocrystals Through the Nanoscale Kirkendall Effect. *Science* **2004,** 304, 711-714.
16. Cabot, A.; Smith, R. K.; Yin, Y.; Zheng, H.; Reinhard, B. M.; Liu, H.; Alivisatos, A. P. Sulfidation of Cadmium at the Nanoscale. *ACS Nano* **2008,** 2, 1452-1458.
17. El Mel, A.-A.; Nakamura, R.; Bittencourt, C. The Kirkendall effect and nanoscience: hollow nanospheres and nanotubes. *Beilstein Journal of Nanotechnology* **2015,** 6, 1348–1361.
18. Wang, W.; Dahl, M.; Yin, Y. Hollow Nanocrystals through the Nanoscale Kirkendall Effect. *Chemistry of Materials* **2013,** 25, 1179-1189.
19. Yu, L.; Yu, X. Y.; Lou, X. W. The Design and Synthesis of Hollow Micro-/Nanostructures: Present and Future Trends. *Advanced Materials* **2018,** 30, 1800939.

20. Yu, Y.; Yin, X.; Kvit, A.; Wang, X. Evolution of Hollow TiO_2 Nanostructures via the Kirkendall Effect Driven by Cation Exchange with Enhanced Photoelectrochemical Performance. *Nano Letters* **2014,** 14, 2528-2535.
21. Lee, Y.-I. Selective transformation of Cu nanowires to Cu_2S or CuS nanostructures and the roles of the Kirkendall effect and anion exchange reaction. *Materials Chemistry and Physics* **2016,** 180, 104-113.
22. Li, Q.; Penner, R. M. Photoconductive Cadmium Sulfide Hemicylindrical Shell Nanowire Ensembles. *Nano Letters* **2005,** 5, 1720-1725.
23. Li, C.; Li, A.; Luo, Z.; Zhang, J.; Chang, X.; Huang, Z.; Wang, T.; Gong, J. Surviving High-Temperature Calcination: ZrO_2-Induced Hematite Nanotubes for Photoelectrochemical Water Oxidation. *Angewandte Chemie International Edition* **2017,** 56, 4150-4155.
24. Yu, L.; Yan, Z.; Cai, Z.; Zhang, D.; Han, P.; Cheng, X.; Sun, Y. Quantitatively in Situ Imaging Silver Nanowire Hollowing Kinetics. *Nano Letters* **2016,** 16, 6555-6559.
25. Xu, L.; Yang, Y.; Hu, Z.-W.; Yu, S.-H. Comparison Study on the Stability of Copper Nanowires and Their Oxidation Kinetics in Gas and Liquid. *ACS Nano* **2016,** 10, 3823-3834.
26. Ding, Y.-L.; Xie, J.; Cao, G.-S.; Zhu, T.-J.; Yu, H.-M.; Zhao, X.-B. Single-Crystalline $LiMn_2O_4$ Nanotubes Synthesized Via Template-Engaged Reaction as Cathodes for High-Power Lithium Ion Batteries. *Advanced Functional Materials* **2011,** 21, 348-355.
27. Colombo, C.; Spirkoska, D.; Frimmer, M.; Abstreiter, G.; Fontcuberta i Morral, A. Ga-assisted catalyst-free growth mechanism of GaAs nanowires by molecular beam epitaxy. *Physical Review B* **2008,** 77, 155326.
28. Küpers, H.; Lewis, R. B.; Tahraoui, A.; Matalla, M.; Krüger, O.; Bastiman, F.; Riechert, H.; Geelhaar, L. Diameter evolution of selective area grown Ga-assisted GaAs nanowires. *Nano Research* **2018,** 11, 2885-2893.
29. Goodyear, J.; Steigmann, G. A. The crystal structure of [alpha]-Ga_2S_3. *Acta Crystallographica* **1963,** 16, 946-949.
30. Jones, C. Y.; Bryan, J. C.; Kirschbaum, K.; Edwards, J. G., Refinement of the crystal structure of digallium trisulfide, Ga_2S_3. In *Zeitschrift für Kristallographie - New Crystal Structures*, 2001; Vol. 216, p 349.
31. Medvedeva, Z. S. Chalcogenides of Elements of Subgroup IIIB of the Periodic System. *Nauka, Moscow* **1968**, 216.
32. Jones, C. Y.; Edwards, J. G. Observation of a Phase Transformation of Ga_2S_3 in a Quartz Effusion Cell above 1230 K by Means of Neutron Scattering. *The Journal of Physical Chemistry B* **2001,** 105, 2718-2724.
33. Barbouth, N.; Berthier, Y.; Oudar, J.; Moison, J. M.; Bensoussan, M. The First Steps of the Sulfurization of III–V Compounds. *Journal of The Electrochemical Society* **1986,** 133, 1663-1666.
34. Pardo, M. P.; Guittard, M.; Chilouet, A.; Tomas, A. Diagramme de phases gallium-soufre et études structurales des phases solides. *Journal of Solid State Chemistry* **1993,** 102, 423-433.
35. Paorici, C.; Zuccalli, G. An open-tube technique to grow Ga_2S_3 crystals. *Journal of Crystal Growth* **1970,** 7, 265-266.
36. Kokh, K. A.; Huang, Z. M.; Huang, J. G.; Gao, Y. Q.; Uralbekov, B.; Panomarev, J.; Lapin, I. N.; Svetlichnyi, V. A.; Lanskii, G. V.; Andreev, Y. M. Study of Ga_2S_3 crystals grown from melt and $PbCl_2$ flux. *Materials Research Bulletin* **2016,** 84, 462-467.
37. Zhou, N.; Gan, L.; Yang, R.; Wang, F.; Li, L.; Chen, Y.; Li, D.; Zhai, T. Nonlayered Two-Dimensional Defective Semiconductor γ-Ga_2S_3 toward Broadband Photodetection. *ACS Nano* **2019,** 13, 6297-6307.

38. Ho, C.-H.; Lin, M.-H.; Wang, Y.-P.; Huang, Y.-S. Synthesis of In2S3 and Ga2S3 crystals for oxygen sensing and UV photodetection. *Sensors and Actuators A: Physical* **2016,** 245, 119-126.
39. Zhang, M.-J.; Jiang, X.-M.; Zhou, L.-J.; Guo, G.-C. Two phases of Ga2S3: promising infrared second-order nonlinear optical materials with very high laser induced damage thresholds. *Journal of Materials Chemistry C* **2013,** 1, 4754-4760.
40. Ho, C.-H.; Chen, H.-H. Optically decomposed near-band-edge structure and excitonic transitions in Ga2S3. *Scientific Reports* **2014,** 4, 6143.
41. Liu, H. F.; Antwi, K. K. A.; Yakovlev, N. L.; Tan, H. R.; Ong, L. T.; Chua, S. J.; Chi, D. Z. Synthesis and Phase Evolutions in Layered Structure of Ga2S3 Semiconductor Thin Films on Epiready GaAs (111) Substrates. *ACS Applied Materials & Interfaces* **2014,** 6, 3501-3507.
42. Liu, H. F.; Ansah Antwi, K. K.; Chua, C. S.; Huang, J.; Chua, S. J.; Chi, D. Z. Epitaxial Synthesis, Band Offset, and Photoelectrochemical Properties of Cubic Ga2S3 Thin Films on GaAs (111) Substrates. *ECS Solid State Letters* **2014,** 3, P131-P135.
43. Spirkoska, D.; Arbiol, J.; Gustafsson, A.; Conesa-Boj, S.; Glas, F.; Zardo, I.; Heigoldt, M.; Gass, M. H.; Bleloch, A. L.; Estrade, S.; Kaniber, M.; Rossler, J.; Peiro, F.; Morante, J. R.; Abstreiter, G.; Samuelson, L.; Morral, A. F. I. Structural and optical properties of high quality zinc-blende/wurtzite GaAs nanowire heterostructures. *Phys Rev B* **2009,** 80, 245325.
44. Sutter, E. A.; Sutter, P. W.; Uccelli, E.; Fontcuberta i Morral, A. Supercooling of nanoscale Ga drops with controlled impurity levels. *Phys Rev B* **2011,** 84, 193303.
45. Yu, L.; Han, R.; Sang, X.; Liu, J.; Thomas, M. P.; Hudak, B. M.; Patel, A.; Page, K.; Guiton, B. S. Shell-Induced Ostwald Ripening: Simultaneous Structure, Composition, and Morphology Transformations during the Creation of Hollow Iron Oxide Nanocapsules. *ACS Nano* **2018,** 12, 9051-9059.
46. Shaikh, H. A. E.; Abdal-Rahman, M.; Belal, A. E.; Ashraf, I. M. Photoconductivity studies of gallium sesquisulphide single crystals. *Journal of Physics D: Applied Physics* **1996,** 29, 466-469.
47. Aono, T.; Kase, K. Green photoemission of α-Ga2S3 crystals. *Solid State Communications* **1992,** 81, 303-305.
48. Dufouleur, J.; Colombo, C.; Garma, T.; Ketterer, B.; Uccelli, E.; Nicotra, M.; Fontcuberta i Morral, A. P-Doping Mechanisms in Catalyst-Free Gallium Arsenide Nanowires. *Nano Letters* **2010,** 10, 1734-1740.
49. Spirkoska, D.; Colombo, C.; Heiss, M.; Abstreiter, G.; Fontcuberta i Morral, A. The use of molecular beam epitaxy for the synthesis of high purity III–V nanowires. *Journal of Physics: Condensed Matter* **2008,** 20, 454225.
50. Meyer, B. Elemental sulfur. *Chem. Rev* **1976,** 76, 367-388.